

UNIVERSITY OF TWENTE

BACHELOR-THESIS

Characterisation of holmium-165 micro-spheres in low-field MRI

Department of biomedical engineering

Luuc de Jongh (s2742276)

Supervisors: dr. ir. F.F.J. Simonis, drs. I. Spenkelink
Committee: dr. ir. F.F.J. Simonis, dr.ir. W.M. Brink, drs. T.J. Snoeijink

July 7, 2024

Abstract

Holmium (Ho) micro-spheres can be imaged in trans-arterial radio-embolisation (TARE) using magnetic resonance imaging (MRI). MRI offers many benefits compared to conventional imaging techniques used in TARE. In previous studies this has been extensively researched using high-field MRI systems of 1.5T and 3T. However, low-field MRI can offer certain advantages over high-field MRI for TARE. To investigate the possibility of using low-field MRI in TARE, holmium micro-spheres are tested in low-field MRI using a 0.5T MRI scanner. Using phantoms containing a range of holmium micro-sphere concentrations, relaxivity r_2^* has been determined at 0.5T 1.5T and 3T. The results at 0.5T show that holmium-microspheres have a significant contrast effect, opening up possibilities for further research into the use of low-field MRI in Ho-TARE.

Contents

1	Introduction	4
2	Theory	5
2.1	Hypothesis	6
3	Materials&Methods	7
3.1	MRI systems	7
3.1.1	Pure devices magspec 0.5T benchtop MRI (UT)	7
3.2	Phantoms	7
3.3	Data-aquisition	8
3.3.1	3T MRI	8
3.4	1.5T MRI	8
3.4.1	0.5T MRI	9
3.5	Data-analysis	10
4	Results	12
5	Discussion	15
6	Conclusion	17

1 Introduction

Trans-arterial radio-embolisation (TARE) is a treatment for irresectable hepatocellular carcinomas (HCC). Diagnosis of HCC often occurs at advanced-stages of the disease where surgical treatment is no longer possible [1] [2]. At advanced stages of HCC patients usually are given only palliative treatment, TARE can provide a potentially curative treatment option for HCC [3]. In the Netherlands alone, every year 100-150 patients with HCC are eligible for TARE [4]. TARE works by injecting radio-isotopes containing microspheres (MS) in the branch of the artery leading to the diseased area, an embolism is induced by the MS lodging themselves in arterioles and capillaries. The radio-isotopes in the MS then irradiate the surrounding tissue. If the MS are deposited at the correct location, the tumor will be irradiated as well. TARE is minimally invasive and requires medical imaging to guide the placement of a catheter to inject the MS in the correct branch of the hepatic artery. Usually X-ray angiography is used for guidance. After the procedure the bio-distribution of the MS and delivered dosage are found by SPECT/CT (combination of single photon emission computed tomography and computed tomography) or (positron emission tomography) PET/CT.

Commonly used radio-isotopes used in TARE are yttrium-90 and holmium-166 (Ho). In recent years holmium-microspheres (Ho-MS) have come into the spotlight in research due to its more favourable properties over yttrium. In particular its paramagnetic properties. Due to this property holmium induces a contrast effect in magnetic resonance imaging (MRI). Thus, instead of using SPECT/CT to find Ho-MS bio-distribution and dosage, it can be done with MRI. MRI-based measurements of dosage and bio-distribution have proven MRI to be a competitive alternative to SPECT/CT [5] [6]. Furthermore, Seppenwoolde et. al. (2005)[7] showed the feasibility of real-time MRI in Ho-TARE, performing catheterization and finding bio-distribution only using MRI. Finally, MRI offers better resolution at equal sensitivity compared to the nuclear imaging techniques used in TARE[8][9]. With the mentioned benefits of MRI for use in Ho-TARE, it is possible to abandon SPECT/CT and X-ray altogether and switch to fully MRI-guided Ho-TARE.

Clinical trials have been performed using MRI to find bio-distribution and dosage of the injected Ho-MS [6] [3], as well as many animal studies [10] [11] [9]. Though as of yet, only high-field MRI ($\geq 1.5T$) has been used in the trials and studies. For intra-operative uses, like in the case of Ho-TARE, the use of low-field MRI (0.1T - 0.5T) becomes more desirable. For Ho-TARE specifically, one of the main advantages of low-field MRI is the bore size. Most low-field MRI systems have a larger bore compared to high-field systems or can even have an open bore [12]. The wider or open bore allows surgical teams more access to the patient while inside. In the case of catheter placement using the aforementioned real-time MRI this better access is a great benefit over the narrow and completely enclosed bore of high-field MRI systems.

To date, there exists no knowledge of Ho-MS being used in low-field MRI. However the characteristics of Ho-MS in low-field need to be known before it can be effectively used for Ho-TARE. For holmium, the main characteristic is relaxivity r_2^* , which reflects the relation between R_2^* and concen-

tration of a certain contrast agent. Physicians can use the known value r_2^* and the measured R_2^* in the organ subjected to Ho-TARE to determine concentrations and subsequently dosage of the deposited Ho-MS. Therefore the goal of this study is to characterize the contrast behaviour of Ho-MS at a field-strength of 0.5T with control measurements at 1.5T and 3T.

2 Theory

As mentioned in the introduction the characteristic of Ho-MS in MRI we are after is r_2^* . r_2^* is the relaxivity and reflects how relaxation rates, in this case the transverse relaxation rates R_2^* , change with respect to i.a. concentration [13]. The r_2^* - values are used in clinical application to determine the distribution, dosage and quantity of Ho-MS using MRI. The R_2^* can be measured by sampling the free induction decay (FID) using a series of gradient echoes (GE). Figure 1 shows an example of the sequence we will be using in the research.

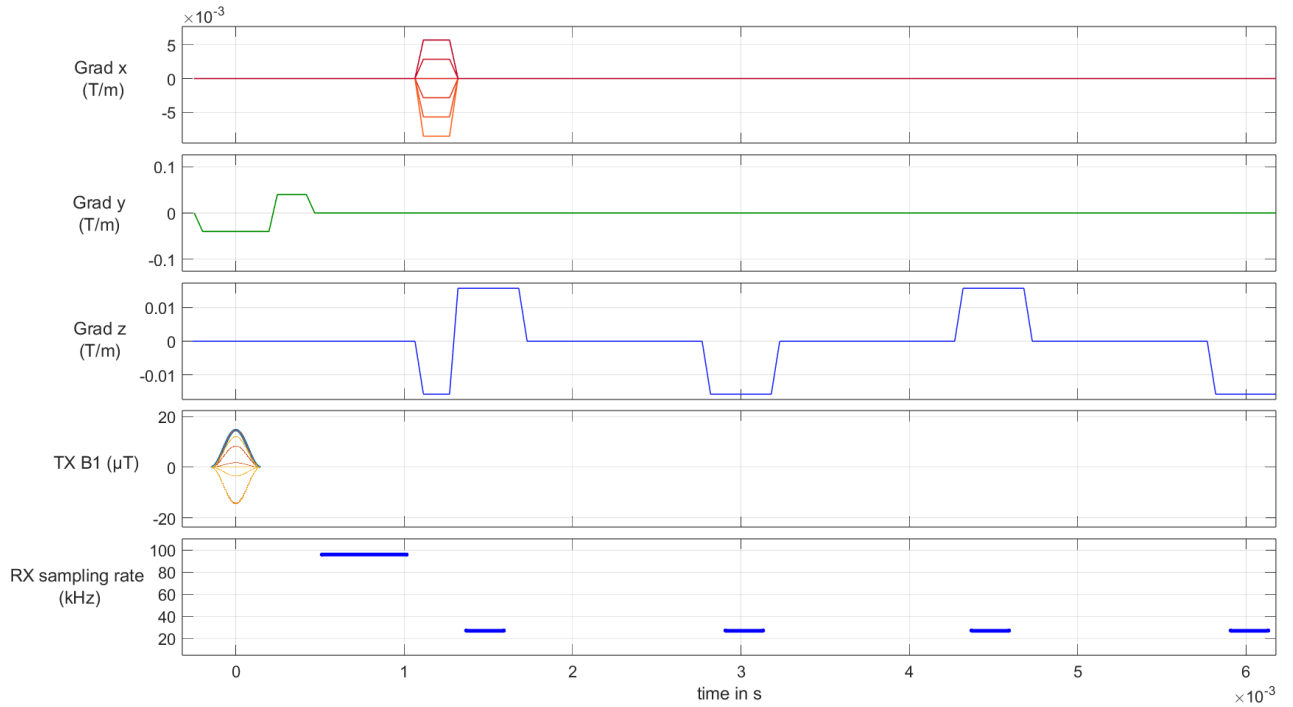


Fig. 1. Example of pulse-sequence that is used for R_2^* -measurement, this specific sequence was used in the measurements done on the 0.5T scanner. The pulse sequence of the 3T and 1.5T measurements will look similar in the sense that the sequence will also be a multi-gradient echo (MGRE)-sequence.

In MRI, ' R ' is a relaxation *rate*, and the variable ' T ' is the relaxation *time*. Relaxation-times and -rates are the inverse of each other.

$$R = \frac{1}{T} \quad (1)$$

R_2^* can be found by sampling the FID using GE's. A mono-exponential fit is drawn through the sampled data. R_2^* can then be found by:

$$S = S(0) * e^{-R_2^*t} + C \quad (2)$$

Where C is the noise-level, t is time, S the magnitude of the signal, $S(0)$ the magnitude of the signal at $t=0$.

Finally, we can find r_2^* by plotting all R_2^* -values against the concentration ($[Ho]$) and drawing a linear regression line. The slope of the linear regression line will be r_2^* .

$$r_2^* = \frac{\Delta R_2^*}{\Delta [Ho]} \quad (3)$$

r_2^* is used in the formula below, describing the effect a certain concentration holmium on the relaxation rates of the tissue. $R_2^{*'} is the relaxation rate of the tissue with a certain $[Ho]$ and R_2^* is the relaxation rate of the tissue without holmium.$

$$R_2^{*' = R_2^* + r_2^* \cdot [Ho] \quad (4)$$

When r_2^* is known, physicians performing TARE using Ho micro-spheres can make a $T2^*$ -map of the treated area. Then the concentration of of the Holmium can be determined in each voxel by using formula 4.

2.1 Hypothesis

Holmium, being part of the lanthanide-group, is paramagnetic. Paramagnetic materials increase the relaxation rates of the surrounding tissue (or in this case the material of the phantom) [14]. The predominant contrast mechanism of holmium is T_2^* [8]. So an increased concentration of Ho-MS present in the phantom will increase the R_2^* we measure.

Since relaxation also depends on field-strength we will have to characterize the effect of Ho-MS in every field-strength we clinically want to use. According to literature R_2^* will increase with magnetic field-strength [12]. The R_2^* -values we find at 0.5T should therefore be lower than their 3T counterparts.

3 Materials&Methods

3.1 MRI systems

Three different MRI systems from the University of Twente (UT) and from Radboudumc Nijmegen are used for measurements: Pure devices magspec 0.5T benchtop MRI (UT), Siemens Magnetom aera 1.5T (UT), and Siemens Magnetom skyra 3T (Radboudumc).

3.1.1 Pure devices magspec 0.5T benchtop MRI (UT)

The original design of this MR is one with 0.55T field strength and a 10mm bore. However, the bore was enlarged to 15mm to accommodate larger samples, which decreased the field strength to 0.5T.

The benchtop MRI system is augmented with a RF-100 rf amplifier, a DC-600 gradient amplifier, and a Drive-L console. The scanner has the capability to heat the magnet to 37°C. The test tubes snugly fit into the bore. So if the phantoms are heated to 37°C before imaging, they will not cool down while inside the MR. Heating the magnet will decrease its field-strength by a few mT, also decreasing the larmor-frequency. However the scanner adjusts its frequency accordingly.

3.2 Phantoms

Clinically relevant Ho concentrations are between 0-1 mg/ml [5] [6][15]. However to find r_2^* concentrations are also chosen outside this range. Data-points further apart will improve accuracy of the fitted line (i.e. the confidence-bands around the linear regression will be smaller). Here we chose concentrations of (0, 0.125, 0.25, 0.5, 0.75, 1, 2, 4, 6, 10) mg/ml of holmium. Holmium-165 PLLA microspheres of diameter 15-60 μm were obtained from Quirem Medical B.V. , the holmium-165 content of the microspheres was 19.71%.

A total of 12 phantoms were made in glass test-tubes of 15 mm diameter and a total volume 20 mL. To make the phantoms, 150 mL of 1.33% agar was prepared and kept between 80 and 100°C. (12.7, 25.4, 50.7, 76.1, 101.4, 202.9, 405.9, 608.8, 1014.7) mg of Ho-MS was added to 6.67 mL of 0.1% phosphate buffered pluronic F68 (a.k.a. Kolliphor P188). This mixture was continually mixed using magnetic stir bars (200-400 rpm) until all clumps of the Ho-MS disappeared. In one phantom, no Ho-MS was added (0 mg/ml). Then, 13.33 mL of 1.33% agarose was added to the pluronic/Ho-MS mixture and left to cool down to 45 °C while continuing to mix. At 45°C, 10 mL of the mixture of pluronic, agarose, and Ho-MS was poured into the test-tube. Due to continuous mixing, it is assumed that the distribution of Ho-MS is homogeneous. In the end, two extra phantoms were created of concentrations 0 and 0.5 mg/ml because the first 0.5 mg/ml phantom was not homogeneously mixed. The first 0.5 mg/ml phantom was excluded from the final results, bringing the amount of phantoms used in the measurements down to 11.



Fig. 2. The fabricated phantoms, from left to right: [0, 0, 0.125, 0.25, 0.5, 0.5, 0.75, 1, 2, 4, 6, 10] mg/ml. Notice the color and opacity change as concentration increases.

3.3 Data-aquisition

3.3.1 3T MRI

For measurements in the 3T MRI scanner, all of the phantoms were placed inside a box and the box was placed in the head array coil in the anterior-posterior/up down direction of the scanner. A liter bag of 0.45% NaCl 2.5% glucose was placed in the head array coil as well to provide enough signal for field shimming. This is because initially the 3T scanner could not shim the field properly because the phantoms did not provide enough signal on their own. The sequence used for the R_2^* measurements was a 2-D fast low angle shot (FLASH). The FID was sampled by 12 gradient echoes ($TE_1 = 1.14$ ms/ $\Delta TE = 1.49$ ms, $TR = 191$ ms). Other scan-parameters were: flip-angle = 33° , slice thickness = 4 mm, voxel size = 2×2 mm, field of view = 384 mm², readout bandwidth = 1532 Hz/pixel.

3.4 1.5T MRI

Measurements at 1.5T were performed in the same manner as the 3T measurements. Scan-parameters were kept as similar as possible to the 3T scan-parameters. The only difference being the echo-time

($TE_1 = 1.31$ ms/ $\Delta TE = 1.68$ ms) and bandwidth (1530 Hz/pixel).



Fig. 3. a: The box with phantoms arranged in the way they went into the 1.5T and 3T MRI system. The numbers written on top of the lids represent the concentrations holmium in the phantoms. 'N' and 'O' at the 0 and 0.5 phantoms indicates the 'new' and 'old' versions of the phantom. As stated, the 'old' 0.5 mg/ml phantom is excluded from the results (see chapter 3.2). b: A 3T MR image of the phantoms, using the mentioned sequence and parameters, in the same order as fig a. Notice how the phantoms of 4-10 mg/ml Ho are not visible and the 2 mg/ml phantom only barely.

3.4.1 0.5T MRI

In the 0.5T MRI-system, the phantoms were imaged one by one because of the bore size. The 0.5T system is operated in MATLAB R2020b (Mathworks, Natick, USA). A preset 'FLASH T2-star' sequence was adjusted to best mimic the sequence used in the 1.5T and 3T measurements. The sequence produced a 2-D map of T_2^* -values of a certain slice in the measured sample (see figure 5). Since the distribution of components in phantom can be assumed homogeneous, it will suffice to only measure the total T_2^* of the slice (i.e. a 0-dimensional measurement). To do this the size of k-space was reduced to 3 by 3 (zero-padding and oversampling ensured that the final image was 12 by 12 pixels). Before taking each measurement, a script was run to automatically set the correct parameters. This included setting the correct frequency, finding the 90 degree RF-pulse duration, and shimming the B0-field. In the 0.5T system, the phantoms were imaged both at room temperature (21°C) as well as 37°C. For the measurements at 37°C the 0.5T magnet was heated to 37°C and the phantoms were placed in a 37°C water bath prior to imaging. The 0 mg/ml phantoms were images twice.

A total of 32 echoes were recorded by sampling the FID using gradient echoes. ($TE_1 = 1.5$ ms/ $\Delta TE = 1.5$ ms). Other parameters were: repetition time = 200 ms, flip angle = 33°, slice thickness = 4 mm, voxel size = 2 × 2 mm.

3.5 Data-analysis

The images acquired from the 1.5T and 3T scanner were loaded into MATLAB R2022b (Mathworks, Natick, USA). A slice was selected and a region of interest (RoI) was drawn within the phantoms in the image: The RoI was selected by clicking on a pixel in the center of the phantom, 21 pixels closest to the selected pixel became the RoI. The mean value of the RoI was plotted against the corresponding TE. A mono-exponential fit to the plotted data-points of the form $S = S(0) \cdot e^{-R_2^* \cdot t} + C$ was applied, to find the R_2^* time constant. Figure 4 shows visually the steps to get from image to signal and R_2^* .

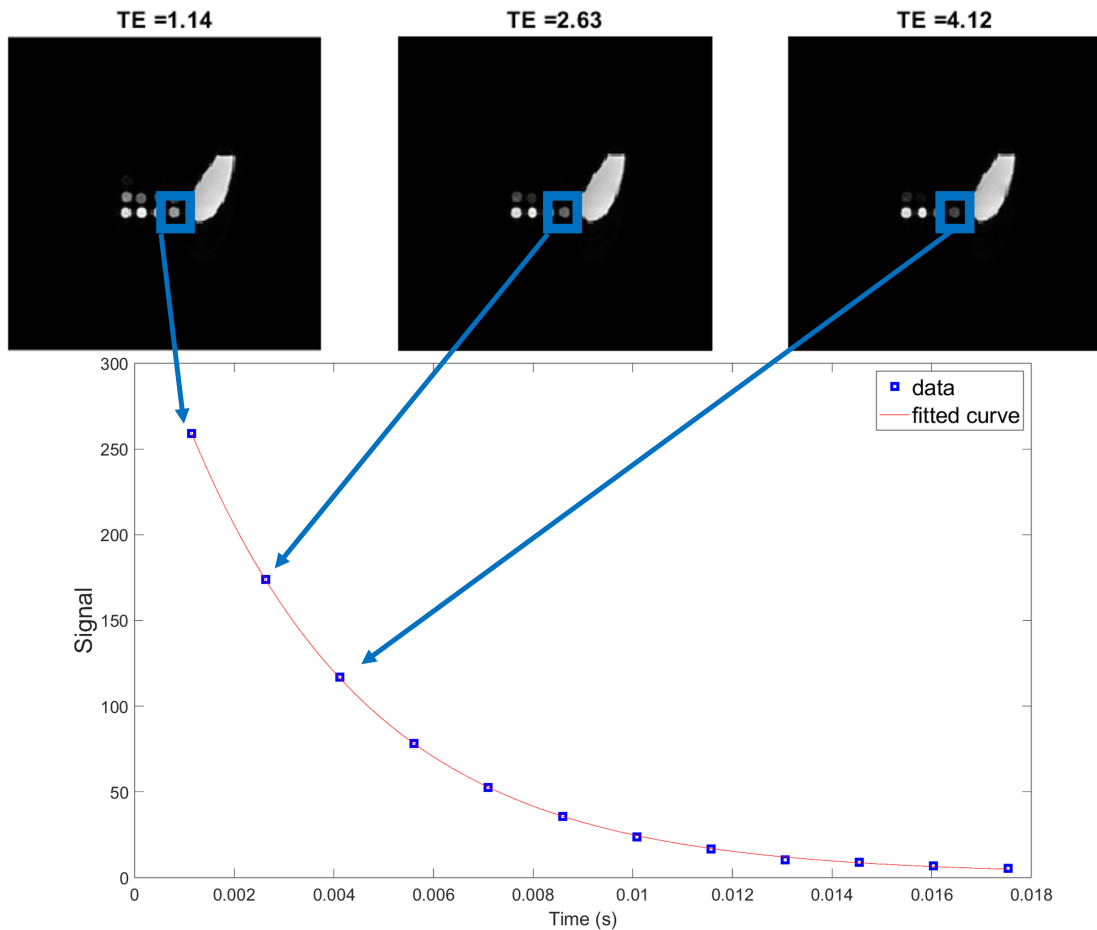


Fig. 4. A slice of the acquired images of the 3T measurements over three echo-times and the data-point (blue squares in the bottom figure) acquired from the echo-times. The red line is the mono-exponential curve fitted to the data-points. In this example the data-points and curve are of the 0.25 mg/ml phantom.

On the 0.5T MR, T_2^* -values were automatically obtained after measurements since scripts for data analysis were already incorporated in the software that controlled the MR. The T_2^* calculated was based on a mono-exponential fit of singular pixel-data. So a separate Matlab program was made to take the mean over the entire bore before performing the fit. Since the phantoms took up the entire bore the the MR, the mean was taken over all pixels. Finally the T_2^* values were converted to R_2^* using formula 1.

Noise was determined by mean value of the last 11 recorded echoes of the 10 mg/ml phantom. Data where the first recorded echo had a $SNR < 3$ were excluded from the final results, which in practice meant that for 3T measurements phantoms of > 2 mg/ml were excluded. At 1.5T phantoms of > 4 mg/ml were excluded. Measurements on 0.5T showed remarkably low noise levels, therefore at 0.5T no data was excluded.

The found R_2^* values of both MR's were plotted against the concentrations Ho-MS in the respective phantoms. A linear fit of the form $R_2^{*'} = a + b \cdot x$ with coefficients a and b was fitted to the obtained data-points. The slope of this line ($\frac{\Delta R_2^*}{\Delta [Ho-MS]}$) is the r_2^* .

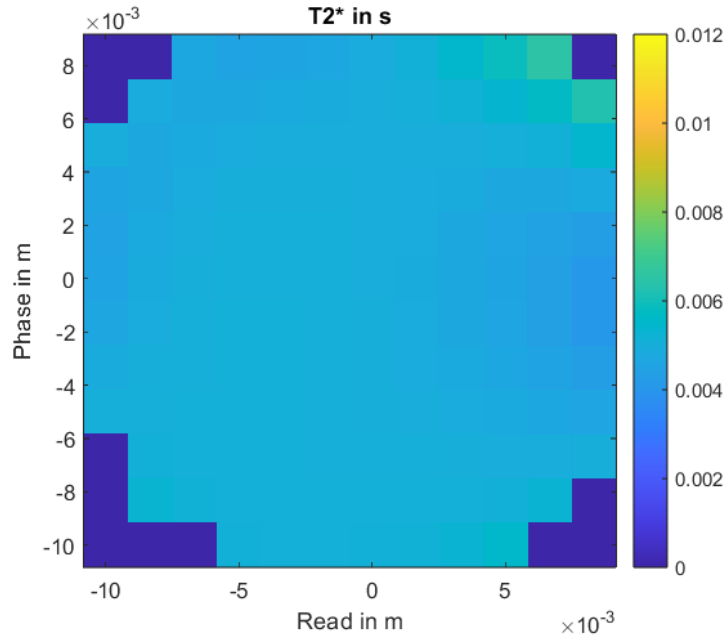


Fig. 5. The image of the 0.75mg/ml phantom created by the 0.5T scanner with the T_2^* FLASH sequence. The dark blue pixels are selected and removed automatically by the Matlab program.

4 Results

The found r_2^* -values are: 1062, 676, 85, and 111 $mg^{-1} s^{-1} ml$ for 3T, 1.5T, 0.5T at 21°C, and 0.5T at 37°C. Images of the exponential fitting to find R_2^* are shown in the appendix. The R_2^* -values themselves are shown in the figures 6-8 as data-points.

All the included 1.5T and 3T R_2^* -values had a R^2 value of >0.98 . All 0.5T R_2^* -values had an NRMSE of ≤ 0.05 .

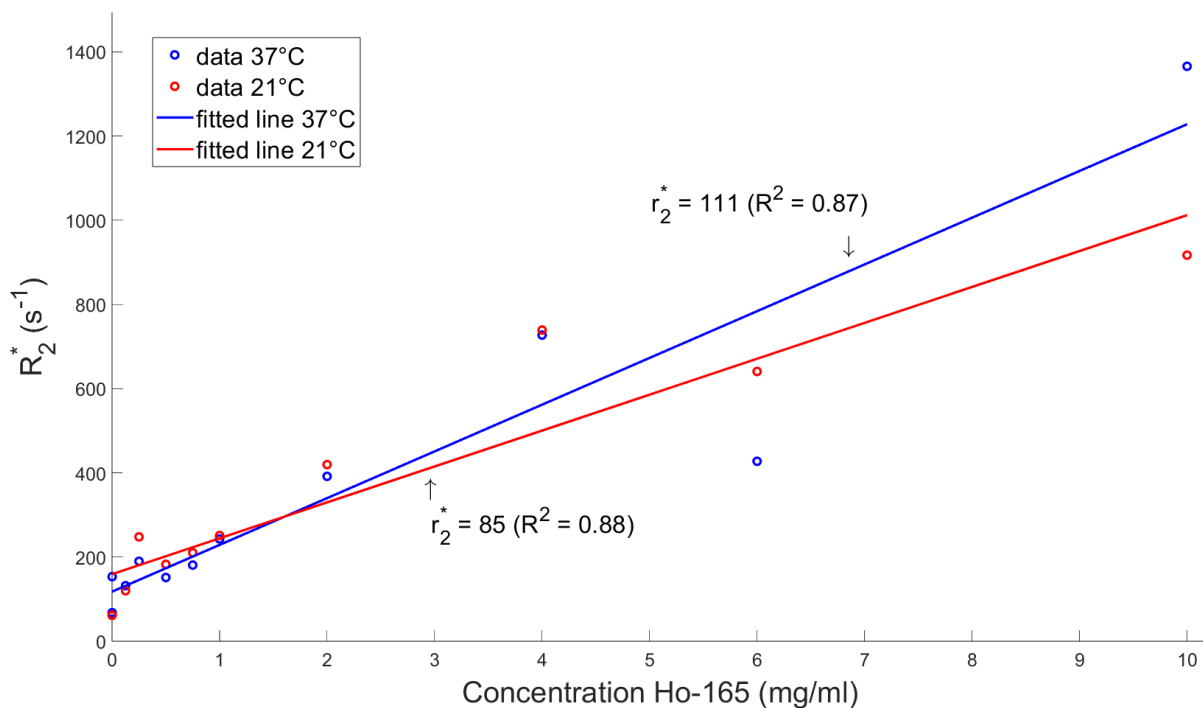


Fig. 6. The difference between room-temperature (21°C) and 37°C. The arrows give the slope of the fitted line in the unit $\frac{ml}{mg \cdot s}$.

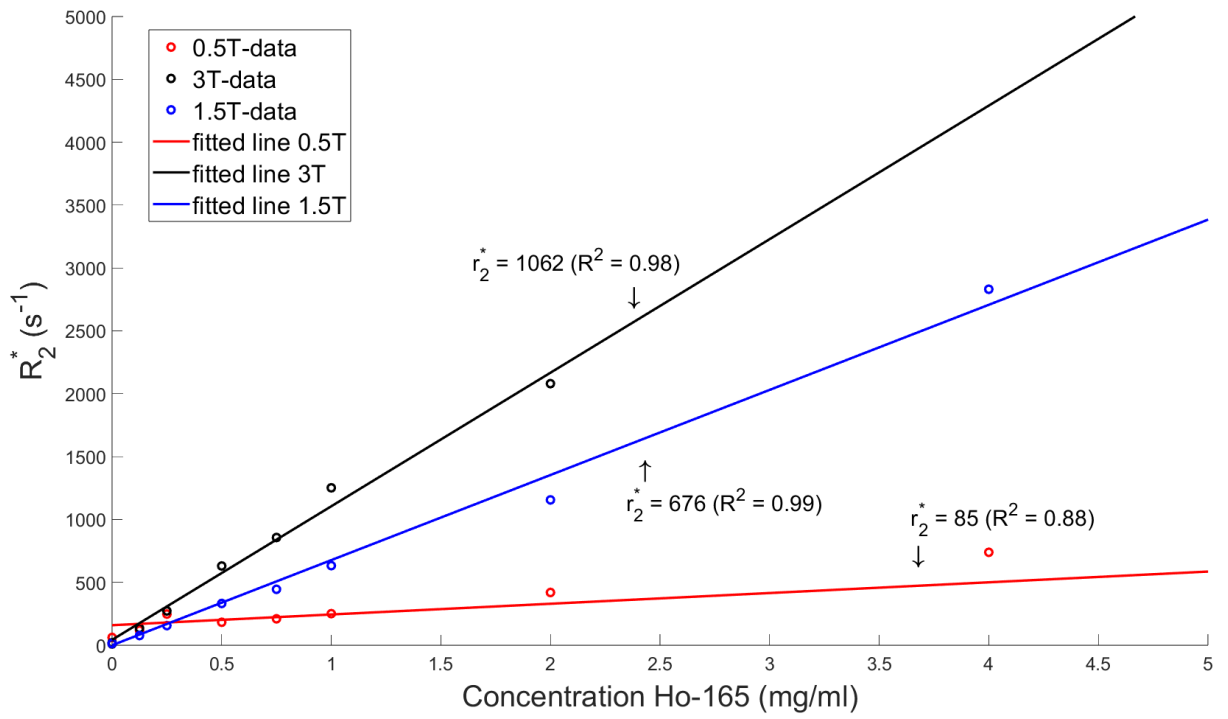


Fig. 7. r_2^* of 3T 1.5T and 0.5T at room temperature (21°C). The arrows give the slope (r_2^*) of the fitted line in the unit $\frac{ml}{mg \cdot s}$.

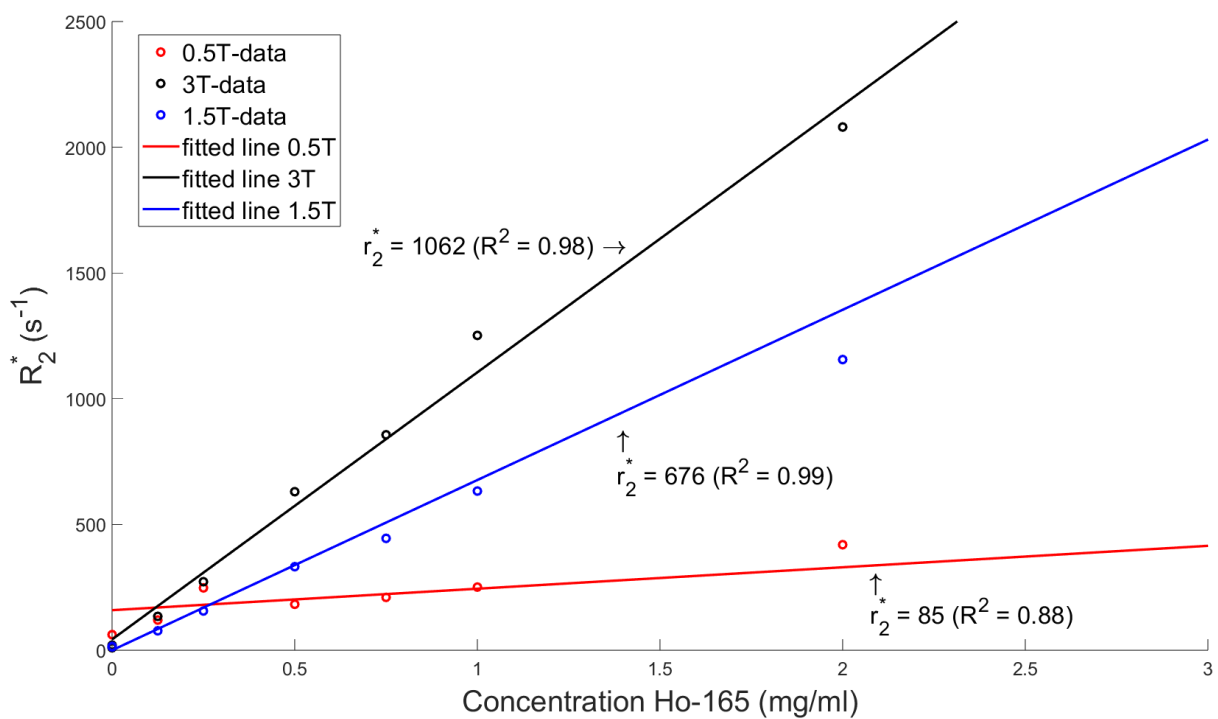


Fig. 8. A zoomed in plot of figure 7. To make data-points at lower concentrations more distinguishable.

5 Discussion

Holmium relaxivity

At first, the found relaxivity of the control-measurements in this study is higher than previously reported values $(180-208)s^{-1} mg^{-1} mL$ at 3T and $(77.2-103)s^{-1} mg^{-1} mL$ at 1.5T [9][8][10][11][16][17]. This explained by the difference in methods, this research reported relaxivity in concentration *holmium* whereas prior research reports it in concentration *micro-spheres*. When we translate our findings to literature by multiplying with the holmium-content (19.71%), our relaxivity becomes 209 and 133 $s^{-1} mg^{-1} mL$ for 3T and 1.5T respectively. Using this measure, r_2^* at 0.5T becomes 17 and 22 $s^{-1} mg^{-1} mL$ for 21°C and 37°C respectively. Both options of expressing relaxivity can be justified. But since holmium content of the Ho-MS differs between batches and/or suppliers, the holmium-content of the Ho-MS should be reported. Being aware of this difference in reporting and ensuring that the correct values are used is essential when applying data for holmium quantification in the Ho-TARE procedure.

Temperature

Relaxivity when used in Ho-TARE procedures, should be based on measurements on 37°C as there is a difference between relaxivities different temperatures. In our findings at 0.5T, r_2^* decreases $26s^{-1} mg^{-1} mL$ between 37°C and 21°C. Which at least qualitatively agrees with the findings of Seevinck et. al. (2008)[17] where r_2^* decreased by $3.1 s^{-1} mg^{-1} mL$ ([Ho-MS]!) between 36°C and 23°C . It is established that temperature has an effect on relaxivity. The best way to avoid erroneous calculated concentrations and subsequent erroneous dosimetry is to find r_2^* at the desired temperature.

Field-strengths

Based on our measurements at the different field-strengths we can find a linear relation between r_2^* and field-strength. Expressing r_2^* as $s^{-1} mg^{-1} mL T^{-1}$, we find r_2^* -values of 170, 450 ,and 354 $s^{-1} mg^{-1} mL T^{-1}$ for 0.5T 1.5T and 3T. Based on this we can conclude that, while r_2^* does decrease significantly, there is no linear decrease in the range of 0.5-3T.

Low-field MRI

This first research into characteristics Ho-MS at low-field MRI showed that R_2^* of holmium can be measured and that the r_2^* can be found. How (or if) the accuracy of dosimetry and bio-distribution of Ho-MS in Ho-TARE is affected by use of lower field-strengths will have to be discovered in further study. In this research, phantoms consisted only of agar and pluronic. So to start, one can modify the phantoms to make the relaxation properties comparable to certain tissues one intends to study

for TARE. The modified phantoms should then be characterized at the relevant temperature(s). Ex-vivo and in-vivo trials using clinical low-field scanners could then compare accuracy of dosimetry and bio-distribution of Ho-MS to methods that are currently in use. Especially the effects of the lower resolution and longer acquisition-time that usually come with low field MRI will need to be researched and considered in Ho-TARE [12][18].

Limitations

In the 0.5T data there are a few outliers in the data-points, reducing the accuracy of r_2^* . Whether this outlier is due to faulty measurement, calibration or fabrication is not known. If the outlier is due to measurement or calibration error, repeated R_2^* -measurements of the phantoms could help mediate the effect of outliers on the linear regression and possibly reveal any errors. Employing S_0 -fitting would also help improve accuracy of R_2^* -values.

Another thing to note about the 0.5T is the very low noise level in our measurements. Which is curious since SNR is expected to decrease with field-strength. Additionally the tabletop scanner used in measurements has a field homogeneity (<10 ppm) which is still larger than most clinical scanners [19]. The low noise level could be due to the low resolution selected at 0.5T, and the significantly reduced acquisition time as a consequence of low resolution could have reduced signal depletion artifacts. New measurements at 0.5T at higher resolutions will have to point this out. Alternatively a sequence could be made for a 0-dimensional R_2^* -measurement.

As observed at field-strengths of 1.5T and 3T, R_2^* -values could not be reliably determined for concentrations holmium of 4 mg/ml and up. Future researches aiming at finding the relaxivity of holmium in a phantom study should pick concentrations up to 4 mg/ml.

6 Conclusion

In this study we have found the of relaxivity r_2^* Ho-165 at 0.5T at room temperature (21°C) as well as 37°C. The 3T and 1.5T measurements served as a control-measurement as r_2^* of holmium at these field-strengths is known.

The found relaxivities of holmium at 0.5T are 85 ($R^2 = 0.88$) $s^{-1} mg^{-1} ml$ and 111 ($R^2 = 0.87$) $s^{-1} mg^{-1} ml$ for 21°C and 37°C respectively. The control measurement at 3T gave a relaxivity of 1062 ($R^2 = 0.98$) $s^{-1} mg^{-1} ml$. Finally at a field strength of 1.5T r_2^* was 676 ($R^2 = 0.99$)

Though the data has outliers which need to be further investigated, based on the decay of apparent transverse magnetisation in the phantoms in our measurements, it is possible to determine R_2^* for holmium-concentrations up to 10 mg/ml at 0.5T. Which is higher than clinically relevant concentrations of Ho (0-1 mg/ml, section 3.2). Opening the possibility for further research into the use of low-field MRI in Ho-TARE.

References

- [1] Llovet JM, Kelley RK, Villanueva A, Singal AG, Pikarsky E, Roayaie S, et al. Hepatocellular carcinoma. *Nature Reviews Disease Primers*. 2021 JAN;7:Not available. Available from: <https://dx.doi.org/10.1038/s41572-020-00240-3>.
- [2] Far BF, Rabie D, Hemati P, Fooladpanjeh P, Hamedanchi NF, Lomer NB, et al. Unresectable Hepatocellular Carcinoma: A Review of New Advances with Focus on Targeted Therapy and Immunotherapy. *Livers*. 2023 MAR;3:121-60. Available from: <https://dx.doi.org/10.3390/livers3010011>.
- [3] Smits ML, Nijsen JF, van den Bosch MA, Lam MG, Vente MA, Huijbregts JE, et al. Holmium-166 radioembolization for the treatment of patients with liver metastases: design of the phase I HEPAR trial. *Journal of Experimental and Clinical Cancer Research*. 2010 JUN;29:Not available. Available from: <https://dx.doi.org/10.1186/1756-9966-29-70>.
- [4] Zorginstituut-Nederland. Holmium-166 radioembolisatie bij hepatocellulair carcinoom. 2022 OCT. Available from: <https://www.zorginstituutnederland.nl/publicaties/standpunten/2022/10/06/holmium-166-radioembolisatie-bij-hepatocellulair-carcinoom>.
- [5] van de Maat GH. MRI-based biodistribution assessment of holmium-166 poly (L-lactic acid) microspheres after radioembolisation. *Eur Radiol*. 2012 SEP;23:827–83. Available from: <https://link.springer.com/article/10.1007/s00330-012-2648-2>.
- [6] Roosen J, van Wijk MWM, Gotby LELW, Arntz MJ, Janssen MJR, Lobeek D, et al. Improving MRI-based dosimetry for holmium-166 transarterial radioembolization using a nonrigid image registration for voxelwise $R2\Delta R_2^*$ calculation. *Medical Physics*. 2022 OCT;50:935-46. Available from: <https://dx.doi.org/10.1002/mp.16014>.
- [7] Seppenwoolde J, Bartels LW, van der Weide R, Nijsen JFW, van het Schip AD, Bakker CJG. Fully MR-guided hepatic artery catheterization for selective drug delivery: A feasibility study in pigs. *Journal of Magnetic Resonance Imaging*. 2005 DEC;23:123-9. Available from: <https://dx.doi.org/10.1002/jmri.20479>.
- [8] Seevinck PR, Seppenwoolde JH, de Wit TC, Nijsen JFW, Beekman FJ, van het Schip AD, et al. Factors Affecting the Sensitivity and Detection Limits of MRI, CT, and SPECT for Multimodal Diagnostic and Therapeutic Agents. *Anti-Cancer Agents in Medicinal Chemistry*. 2007 MAY;7:317-34. Available from: <https://dx.doi.org/10.2174/187152007780618153>.
- [9] Nijsen JFW, Seppenwoolde JH, Havenith T, Bos C, Bakker CJG, van het Schip AD. Liver Tumors: MR Imaging of Radioactive Holmium Microspheres—Phantom and Rabbit Study. *Radiology*. 2004 MAY;231:491-9. Available from: <https://dx.doi.org/10.1148/radiol.2312030594>.

- [10] Seppenwoolde J, Nijsen JFW, Bartels LW, Zielhuis SW, van het Schip AD, Bakker CJG. Internal radiation therapy of liver tumors: Qualitative and quantitative magnetic resonance imaging of the biodistribution of holmium-loaded microspheres in animal models. *Magnetic Resonance in Medicine*. 2004 DEC;53:76-84. Available from: <https://dx.doi.org/10.1002/mrm.20320>.
- [11] Seevinck PR, van de Maat GH, de Wit TC, Vente MAD, Nijsen JFW, Bakker CJG. Magnetic Resonance Imaging-Based Radiation-Absorbed Dose Estimation of ^{166}Ho Microspheres in Liver Radioembolization. *International Journal of Radiation Oncology*Biophysics*. 2012 JUL;83:e437-44. Available from: <https://dx.doi.org/10.1016/j.ijrobp.2011.12.085>.
- [12] Marques JP, Simonis FFJ, Webb AG. Low-field MRI: An MR physics perspective. *Journal of Magnetic Resonance Imaging*. 2019 JAN;49:1528-42. Available from: <https://dx.doi.org/10.1002/jmri.26637>.
- [13] Elster AD. Relaxivity. Available from: <https://mriquestions.com/what-is-relaxivity.html>.
- [14] Bushberg JT, Boone JM. *The Essential Physics of Medical Imaging*. Lippincott Williams Wilkins; 2011.
- [15] van de Maat GH, de Leeuw H, Seevinck PR, van den Bosch MAAJ, Nijsen JFW, Bakker CJG. Simultaneous R_2^* , R_2 , and R_2' quantification by combining S_0 estimation of the free induction decay with a single spin echo: A single acquisition method for R_2 insensitive quantification of holmium-166-loaded microspheres. *Magnetic Resonance in Medicine*. 2014 MAR;73:273-83. Available from: <https://dx.doi.org/10.1002/mrm.25138>.
- [16] van de Maat GH, Seevinck PR, Bos C, Bakker CJG. Quantification of holmium-166 loaded microspheres: Estimating high local concentrations using a conventional multiple gradient echo sequence with S_0 -fitting. *Journal of Magnetic Resonance Imaging*. 2012 JAN;35:1453-61. Available from: <https://dx.doi.org/10.1002/jmri.23593>.
- [17] Seevinck PR, Seppenwoolde J, Zwanenburg JJM, Nijsen JFW, Bakker CJG. FID sampling superior to spin-echo sampling for T_1 -based quantification of holmium-loaded microspheres: Theory and experiment. *Magnetic Resonance in Medicine*. 2008 NOV;60:1466-76. Available from: <https://dx.doi.org/10.1002/mrm.21785>.
- [18] Elster AD. Low-field Disadvantages. Available from: <https://mriquestions.com/disadvantages.html>.
- [19] Koch KM, Rothman DL, de Graaf RA. Optimization of static magnetic field homogeneity in the human and animal brain in vivo. *Progress in Nuclear Magnetic Resonance Spectroscopy*. 2009 FEB;54:69-96. Available from: <https://dx.doi.org/10.1016/j.pnmrs.2008.04.001>.

Appendix

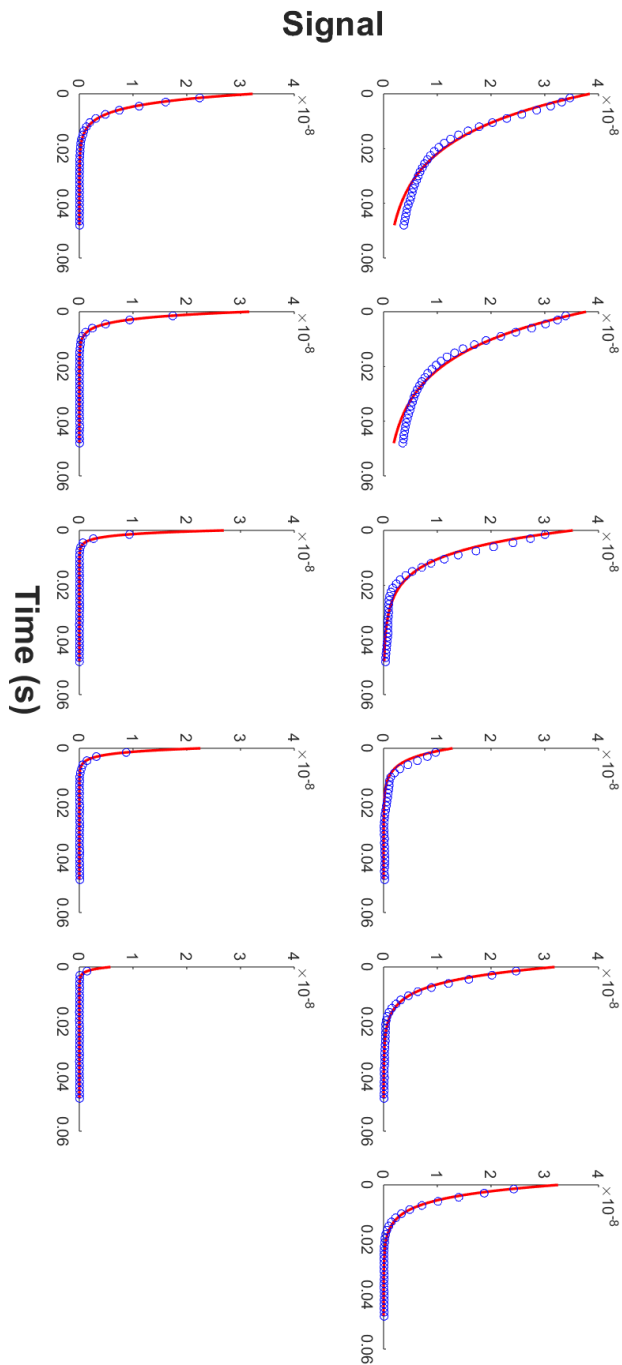


Fig. 9. Exponential fits (red line) made through the recorded echoes (blue dots) at 0.5T. From left to right top to bottom [0 ,0 ,0.125 ,0.25, 0.5, 0.75, 1, 2, 4, 6, 10] mg/ml. The 'old' 0.5mg/ml phantom has been removed from the set

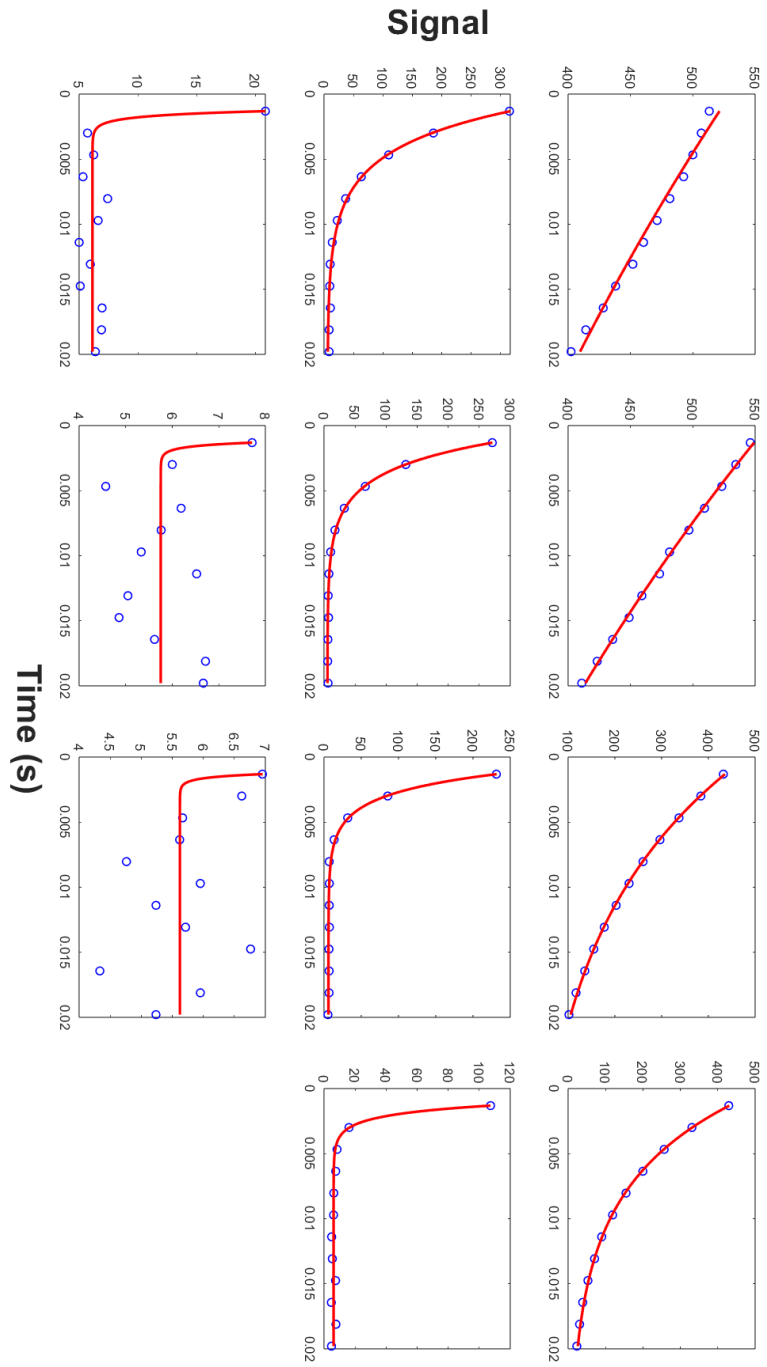


Fig. 10. Exponential fits (red line) made through the recorded echoes (blue dots) at 1.5T. From left to right top to bottom [0 ,0 ,0.125 ,0.25, 0.5, 0.75, 1, 2, 4, 6, 10] mg/ml. The 'old' 0.5mg/ml phantom has been removed from the set

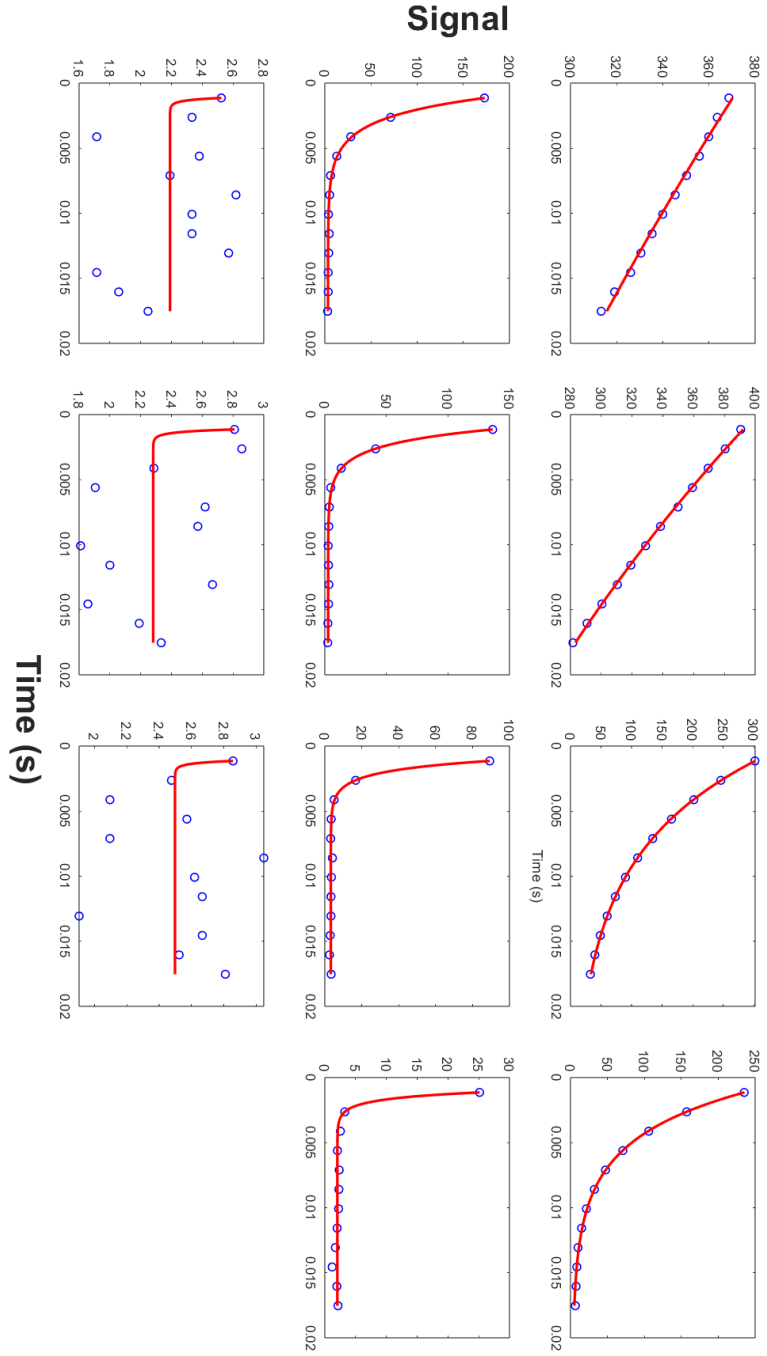


Fig. 11. Exponential fits (red line) made through the recorded echoes (blue dots) at 3T. From left to right top to bottom [0 ,0 ,0.125 ,0.25, 0.5, 0.75, 1, 2, 4, 6, 10] mg/ml. The 'old' 0.5mg/ml phantom has been removed from the set